Mechanical Engineering Advances 2025, 3(2), 2878.
https://doi.org/10.59400/mea2878

Article

Semi-analytical solution for nonlinear Von Kármán swirling fluid flow via the hybrid analytical and numerical method

Ali Ahmadi Azar

Department of Mechanical Engineering, North Tehran Branch, Islamic Azad University, Tehran, Iran; aliahmadiazar.mech@gmail.com, a.ahmadi.azar@iau-tnb.ac.ir

CITATION

Ahmadi Azar A. Semi-analytical solution for nonlinear Von Kármán swirling fluid flow via the hybrid analytical and numerical method. Mechanical Engineering Advances. 2025; 3(2): 2878. https://doi.org/10.59400/mea2878

ARTICLE INFO

Received: 1 March 2025
Accepted: 1 April 2025
Available online: 10 April 2025

Abstract: This study investigates the nonlinear and classical problem of Von Kármán's viscous swirling fluid flow caused by a single rotating disk. Despite over a century since this problem was first introduced, recent advancements enable more accurate calculations and practical results than previously possible. The core innovation of this paper lies in the application of the Hybrid Analytical and Numerical method (HAN method), which facilitates the derivation of a semi-analytical solution to complex nonlinear differential equations. The HAN method combines numerical and analytical approaches to solve nonlinear problems. Initially, the system of nonlinear differential equations is solved using an arbitrary numerical method. The numerical solution then aids in extracting the analytical solution, which can take forms such as polynomial solutions with constant and unknown coefficients. Since boundary conditions lack the capacity to generate a sufficient number of algebraic equations, the numerical solution provides the additional required equations. The flexibility of the HAN method stems from its ability to leverage various numerical methods, making it a robust approach for solving nonlinear differential equations. Using this methodology, the Von Kármán problem is analytically calculated with remarkable accuracy. Furthermore, this study provides highly precise calculations of several physical and practical outputs, including the thickness of the layer, the slope of flow lines at the wall in the peripheral direction, the peripheral component of wall shear stress, the moment on one side of the wetted disk, the dimensionless moment coefficient for both sides of the disk, Reynolds number as a function of the disk's finite radius, volume flux, and mechanical power. This research contributes to two main perspectives: first, the mathematical aspect, which demonstrates the ability of the HAN method to solve various nonlinear problems; second, the practical-physical perspective, showcasing the enhanced accuracy and reliability of the obtained results in analyzing fluid flow mechanics.

Keywords: Von Kármán swirling viscous flow; semi-analytical solution; the Hybrid Analytical and Numerical Method; the HAN-method

1. Introduction

In fluid mechanics, rotating flows are a common phenomenon due to many industrial, mechanical, and environmental applications such as rotary pumps, fans, turbines, boilers and chemical storage, cyclone separators, and rotating disks of nuclear reactors, and have attracted considerable attention [1]. The Von Kármán rotational viscous flow is a well-known classical problem in fluid mechanics, and Von Kármán [2], in this famous problem, investigated the viscous fluid flow resulting from the rotation of a disk in such a way that the fluid far from the disk is stationary and introduced new variables called similarity transformations that allowed PDEs to be converted to ODEs, which later were called the Von Kármán similarity variables. More recent results were obtained by the Cochran [3] with a modification of the Von Kármán

problem. Von Kármán's answers contained errors that Cochran corrected. Bödewadt [4] was also the first to present a problem in which the disk is stationary and the fluid flow is the result of fluid rotation from a distance away from the disk. Just like rotating the coffee in the cup, the bottom of the cup is fixed, but by rotating the coffee, the fluid rotation is transferred everywhere. This form of fluid flow was later called Bödewadt flow, and Fettis [5] was one of the first to use Bödewadt flow. Rogers and Lance [6] studied the case where the fluid rotates at infinity with different uniform velocities in the same direction as the disc velocity, and the results of Von Kármán [2] and Bödewadt [4] were obtained in special cases. Batchelor [7] studied the problem in which the fluid is flowing due to the rotation of the disc with different uniform velocities and also different velocities of the fluid at certain distances. Specific distances mean both the infinite distance, which means the distance far from the disk, and the specified distances or close to the disk. Batchelor [7] studied the problem in which the fluid flows with different uniform velocities at certain distances and the rotation of the disk with different uniform velocities. Certain distances mean both infinite distance, which means far from the disk, and certain distances or close to the disk. Benton [8] extended Von Kármán's rotating disc problem to a transient problem and also solved Von Kármán's steady-state problem for more accuracy. Zandbergen and Dijkstra [9] presented a review paper of the studies [3,5,6,8], and also, in the mentioned studies [3–8], Von Kármán similarity variables have been used to convert the PDEs of the governing equations into ODEs. Tien and Tsuji [10] made theoretical inferences using numerical methods for the temperature distribution and heat transfer results due to the forced laminar motion on a non-isothermal rotating plate. Evans and Greif [11] analyzed the flow between two parallel plates. One is porous, unheated, and stationary, and the other is impermeable, heated, and rotating. The PDEs were reduced into a set of nonlinear ODEs via similarity transformation, and then the ODEs were solved numerically. By using the perturbation method, Sharma [12] investigated the fluid flow that is constrained by two infinitely swirling plates for three cases: the first case is when the plates have the same angular velocity, the second case is when the plates have different angular velocities, and the third case is when one plate has angular velocity and the other is at rest. Kumari et al. [13] investigated the asymmetric motion produced by the flow of a conductive fluid in a rotating infinite plate. There is also a magnetic field perpendicular to the plane. Similarity transformation is also considered for reducing the governing equations into a set of ODEs and solved numerically by the shooting method. Ozetkin and Brown [14] studied the viscometric motion of the viscoelastic fluid that is between two swirling parallel disks. Deshpande and Ghosh [15] studied the unsteady fluid flow that was caused by an infinite swirling disk numerically. Choudhury and Das [16] investigated the fluid motion that is constrained between two spinning disks, which has the elastic-viscous property. Shevchuk and Buschmann [17] investigated the fluid that co-rotates with the spinning disk. The governing equations were reduced into a set of ODEs by the similarity transformation, and then the ODEs were solved numerically. The heat transfer problem studied by aus der Wiesche [18] when the air flow passes from a swirling disk numerically. Hayat et al. [19] studied the MHD swirling flow of a fluid in a porous medium where the fluid model obeys the modified Darcy's law. The Hall effect was also considered for this model, and finally, ODEs were solved by the HAM. Yang and Liao [20] solved the

classical problem of Von Kármán [2] analytically by the HAM and compared the analytical results with the previous numerical solutions. Attia [21] investigated non-Newtonian, incompressible, and viscous fluid and considered the motion of this fluid on a stretchable swirling disk. The governing equations of the steady-state fluid flow were reduced into nonlinear ODEs, and they were solved numerically by the finite difference method. Bessaïh et al. [22] analyzed the stability of the swirling flow of liquid metal between two disks filled in a cylindrical chamber. One of the disks rotates at a certain temperature, while the other remains stationary at a different temperature. The governing equations were in PDE form and were solved numerically through FVM. Rahman and Postelnicu [23] investigated the thermal effects of the fluid flow caused by a rotating disk with a temperature different from the environment and then solved the equations numerically. Similar to Yang and Liao [20], Abdou [24] solved the classical problem of Von Kármán [2] analytically with the homotopy perturbation method. Turkyilmazoglu [25] investigated a boundary layer problem that is concerned with the motion of the fluid created by the rotation of a disk that disk injection or suction ability. Turkyilmazoglu [26] studied the fluid boundary layer that was caused by a swirling disk in a steady-state condition and solved by the analytical method of homotopy analysis. The results of the homotopy analysis technique compared with the numerical method of Runge-Kutta. Rashidi et al. [27] analyzed the second law of thermodynamics for nanofluid flow on a rotating disk. The vertical magnetic field is also presented in the problem. The governing equations were reduced to ODEs by converting to similarity, and then the ODEs were solved numerically. The study of Alam et al. [28] concerned the transient forced convective fluid flow that resulted from a swirling disk. The particles of fluid flow were assumed to be of micro size. The governing equations were transformed into the ODEs by the similarity transformation and solved numerically. Hayat et al. [29] analyzed the problem of ferrofluid flow bounded by two parallel planes, which are infinite planes but have different angular velocities. The governing equations were converted to ODEs by similarity transformation and converted to ODEs by the HAM. Doh et al. [30] studied micropolar fluid flow created by a rotating plate. A magnetic field perpendicular to that plane is also applied. The PDEs of the governing equations were converted into ODEs using similarity transformation and solved numerically. Das and Sahoo [31] studied the Reiner-Rivlin fluid flow problem confined between two parallel rotating infinite disks. The governing equations were transformed into a set of ODEs by similarity transformation and then solved using the homotopy method. Kumar et al. [32] carried out a numerical investigation on the problem of rotating flow of a Rainer-Rivlin fluid, where the surface of a rotating disk satisfies the Navier velocity slip condition in the presence of a magnetic field. Temperature jump conditions because of incomplete liquid-solid energy matching are also considered. Visuvasam and Alotaibi [33] did analytical research on the problem related to the rotating Von Kármán flow of a viscous incompressible fluid due to a rotating disk electrode. The governing equations are based on four nonlinear coupled differential equations and were solved by homotopy analysis. Ali et al. [34] investigated the problem of non-transient and incompressible convective flow of Rainer-Rivlin nanofluid through a rotating disk with different slip conditions. The governing equation was reduced to five coupled nonlinear ODEs with the help of similarity variables and solved through the BVP4c numerical method. In a

recent study, a new semi-analytical method known as the Hybrid Analytical and Numerical Method (HAN method) was introduced for the first time by Jalili et al. [35]. This method was employed to solve the equations addressing the heat and mass transfer of a viscous, incompressible, laminar axisymmetric flow of a micropolar fluid in the presence of a magnetic field, constrained between two stretchable disks. To enhance the credibility and relevance of the HAN method, the article incorporates references to additional published studies [36–39] where this method has been effectively applied to solve governing equations similar to those addressed in the current study. In a recent study, the Hybrid Analytical and Numerical Method (HAN method), initially introduced by A. Ahmadi Azar, was applied as a semi-analytical technique to analyze the non-transient forced motion of a non-Newtonian MHD Reiner-Rivlin viscoelastic fluid confined between two plates [36]. The model included the presence of a magnetic field. The governing equations, initially in partial differential equation (PDE) form, were transformed into a set of ordinary differential equations (ODEs) using the Von Kármán similarity variables. The HAN method was then applied to solve the ODEs and their associated boundary conditions analytically. For validation, the results obtained from the HAN method were compared with those derived from the Homotopy Perturbation Method (HPM) and the numerical Runge-Kutta technique. Additionally, new quantitative results were extracted from the HAN solutions. Another study explored the steady, laminar, incompressible, and two-dimensional flow of a micropolar fluid between two disks [37]. In this analysis, the upper disk was assumed to be porous, while the lower one was non-porous. Body forces and body couples were disregarded, and the flow was considered fully developed. The governing equations were transformed into a set of ordinary differential equations (ODEs) using Von-Kármán's similarity variables. Since these ODEs had not been previously solved analytically, the Modified Akbari-Ganji Method (Modified AGM) and the Hybrid Analytical and Numerical Method (HAN method) were employed to obtain semi-analytical solutions. A primary novelty of the study was the application of these methods to achieve such solutions, although much of the innovation lay in the physical insights derived from the analytical results. The impacts of various slip coefficients, Reynolds numbers, and micropolar parameters—such as vortex viscosity, spin gradient viscosity, and microinertia density—were examined on profiles of normal velocity, streamwise velocity, and microrotation. The validity of the solutions was demonstrated through comparison with previously published results, with both methods producing nearly identical findings in all cases, indirectly confirming the reliability of the results. In another study [38], the Hybrid Analytical and Numerical Method (HAN method) was employed to solve nonlinear coupled ordinary differential equations (ODEs), investigating the effects of structural changes such as variations in the stretching rate and the distance between two disks on key physical quantities. The study demonstrated that an increased stretching rate significantly raised the temperature and Nusselt number, while increasing the distance between the disks led to a substantial reduction in microrotation and wall couple stress. By redefining parameters such as the magnetic parameter, Eckert number, stretching Reynolds number, and micropolar parameters, the research focused on analyzing physical quantities impacted by these structural changes. The findings were validated through comparisons with prior studies, ensuring accuracy and reliability. In another

study [39], the HAN method was used to find an exact solution for the Von Kármán swirling viscous fluid flow caused by a rotating disk with uniform suction. Three cases were considered: swirling flow at infinity with directions opposite and similar to the angular velocity of the rotating disk, no swirling flow with suction on the disk's surface, and both swirling flow and suction on the disk. The findings revealed that when the angular velocity of the fluid at infinity decreased relative to the angular velocity of the disk, the skin friction coefficient reached its maximum, while an increase in fluid angular velocity led to its reduction. For the second case, higher surface suction caused an increase in the skin friction coefficient, making it greater on porous disks than on non-porous ones. Additionally, under specific conditions where both swirling flow and suction were absent, the pressure distribution depended solely on the distance above the disk. These results demonstrated the effectiveness of the HAN method in solving complex fluid flow scenarios and analyzing skin friction and pressure distributions in varying conditions. However, the HAN method is not limited to studies related to swirling flow due to the one or two disks [40–49]. Xu and Liao [50] studied the unsteady motion of a conducting viscous fluid driven by a rapidly spinning infinite disk. They employed the HAM to derive analytical solutions, first converting the governing Navier-Stokes equations into a system of nonlinear PDEs through novel similarity transformations. Their approach yielded convergent series solutions that remained valid across all time scales ($0 \leq \tau < \infty$) and throughout the entire flow domain ($0 \leq \eta < \infty$). This represented a significant advancement, as such comprehensive analytical solutions hadn't been achieved before. The work also quantified how magnetic field strength influenced the fluid's velocity characteristics. Mehmood et al. [51] employed the HAM to obtain analytical solutions for unsteady Von Kármán swirling flow induced by a suddenly rotating infinite disk, presenting complete closed-form solutions valid across all time ($0 \leq \tau \leq \infty$) and space ($0 \leq \eta \leq \infty$). Their results showed excellent agreement with Yang and Liao's [20] steady-state solution ($\tau \to \infty$) and revealed that flow velocity gradually increases over time until reaching steady-state conditions, while the hydrodynamic boundary layer thickness initially grows before stabilizing at a constant value. These analytical solutions serve as valuable benchmarks for numerical simulations in applications like helicopter rotor aerodynamics, rotating electrochemical systems, and turbine blade flow analysis. Sadiq [52] investigated unsteady viscous flow over a decelerating, rotating, stretchable disk. The study transformed the governing nonlinear partial differential equations into ordinary differential equations using similarity transformations, then solved them analytically using the HAM. The research demonstrated the convergence of HAM solutions and validated results through comparison with numerical solutions. Key findings included the effects of disk stretching and unsteadiness parameters on flow characteristics. The work provides analytical solutions for this complex rotating flow system with practical applications in rotating machinery and industrial processes involving stretchable surfaces. Finally, the analytical studies about the transient fluid flows due to one disk are developed by Bég et al. [53]. They investigated transient nanofluid flow around a time-dependent spinning sphere for coating applications, transforming the governing equations into a ninth-order nonlinear system using similarity variables. They solved this computationally challenging problem using the

HAM, verifying results with Adomian decomposition (ADM), and analyzed how acceleration, rotation, Brownian motion, thermophoresis, Lewis and Prandtl numbers affect shear stress, heat/mass transfer, and boundary layer behavior. The study demonstrated HAM's effectiveness in handling this complex nanofluid system, providing accurate solutions with good convergence that advance understanding of rotating-body nanofluid dynamics for industrial applications.

In this study, the classical problem of Von Kármán [2] that concerned the three-dimensional steady, laminar, axially-symmetric viscous fluid flow caused by an infinite radius disk with uniform angular velocity about z-axis. The partial governing differential equations of the problem are in a cylindrical coordinate system, and they are reduced into a system of coupled nonlinear ODEs with the help of Von Kármán similarity variables. Despite all these years since the introduction of this problem, Von Kármán's equations have not been approximated with great accuracy. Since the introduction of this problem in fluid mechanics, it has been solved many times by numerical methods [2,3]. But with the computers available to researchers today, these equations can be obtained with much greater accuracy than previously published numerical results. Also, various analytical solutions were presented [20,24], but the weak points of these analytical solutions are the large number of solution sentences. Therefore, according to these weaknesses of published analytical and numerical solutions, it is possible to compensate for the deficiencies of the past, and for this purpose, the HAN method is one of the most appropriate methods to achieve an accurate analytical solution. So, the innovation of this article is to show the application of the semi-analytical method of HAN in approximating the equations of a classic problem analytically with high accuracy.

2. Methodology

This part of the article belongs to the derivation of dimensionless Von Kármán's equations from the governing equations of conservation of mass and momentum in three directions by using the similarity variable introduced by Von Kármán [2]. **Figure 1** shows a geometric schematic of the problem, which represents a three-dimensional flow and shows the rotational motion of the fluid resulting from the uniform swirling of a disk with infinite radius.

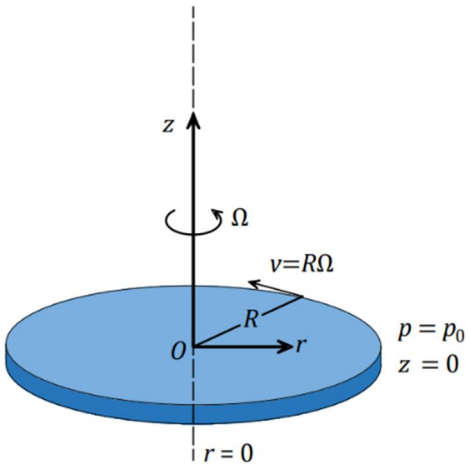

Figure 1. Geometric schematic of the problem.

In this problem and according to **Figure 1**, the disk is rotating with a constant angular velocity of Ω, and due to the viscosity of the fluid and the lack of fluid slip on the surface, the fluid rotates with the disk and causes a rotational flow. According to the figure, it can be said that the highest rotational velocity is near the disk, and the rotational velocity causes the rotating fluid to be pushed out along the radius of the disk, which is denoted by r. The fluid pushed around the disk creates a vacuum, and the vacuum itself causes fluid suction along the disk's axis of rotation. So, it can be said that the rotation of the disk is like a three-dimensional pump that sucks the fluid from above and pushes it along the radius of the disk. The steady governing partial differential equations of momentum and mass in the cylindrical coordinate system for the laminar, axially symmetric, viscous, and incompressible fluid flow are as follows:

The equation of conservation of mass [20,24]:

$$\frac{1}{r}\frac{\partial(rV_r)}{\partial r}+\frac{1}{r}\frac{\partial V_\theta}{\partial \theta}+\frac{\partial V_z}{\partial z}=0 \tag{1}$$

The equation of conservation of momentum along r-axis [20,24]:

$$V_r\frac{\partial V_r}{\partial r}+V_z\frac{\partial V_z}{\partial z}-\frac{V_\theta^2}{r}=\nu\left[\frac{\partial^2 V_r}{\partial r^2}+\frac{1}{r}\frac{\partial V_r}{\partial r}+\frac{\partial^2 V_r}{\partial z^2}-\frac{V_r}{r^2}\right]-\frac{1}{\rho}\frac{\partial p}{\partial r} \tag{2}$$

The equation of conservation of momentum along θ-axis [20,24]:

$$V_r\frac{\partial V_\theta}{\partial r}+V_z\frac{\partial V_\theta}{\partial z}+\frac{V_\theta V_r}{r}=\nu\left[\frac{\partial^2 V_\theta}{\partial r^2}+\frac{1}{r}\frac{\partial V_\theta}{\partial r}+\frac{\partial^2 V_\theta}{\partial z^2}-\frac{V_\theta}{r^2}\right] \tag{3}$$

The equation of conservation of momentum along z-axis [20,24]:

$$V_r\frac{\partial V_z}{\partial r}+V_z\frac{\partial V_z}{\partial z}=\nu\left[\frac{\partial^2 V_z}{\partial r^2}+\frac{1}{r}\frac{\partial V_z}{\partial r}+\frac{\partial^2 V_z}{\partial z^2}\right]-\frac{1}{\rho}\frac{\partial p}{\partial z} \tag{4}$$

where ρ is fluid density, ν is the kinematic viscosity, r, θ, and z are cylindrical coordinate components, p is the pressure, V_θ, V_r, and V_z are the velocity components along the azimuthal, radial, and axial axes, respectively. The boundary conditions of Equations (1)–(4) are as follows [20,24]:

$$\begin{gathered} V_\theta = r\Omega, V_r = V_z = 0, p = p_0, \text{when } z = 0 \\ V_r = V_z = 0, \text{when } z = +\infty \end{gathered} \tag{5}$$

where the Ω is the constant angular velocity. With the help of the following similarity variables that were introduced by Von Kármán [2,20,24,54]:

$$\begin{gathered} V_r = r\Omega F(\xi) \\ \xi = (\Omega/\nu)^{1/2} z \\ V_\theta = r\Omega G(\xi) \\ V_z = (\nu\Omega)^{1/2} H(\xi) \\ p = p_0 + \rho\nu\Omega P(\xi) \end{gathered} \tag{6}$$

where $F(\xi)$ is similarity radial velocity, $G(\xi)$ is similarity azimuthal velocity, $H(\xi)$ is the similarity axial velocity, $P(\xi)$ is the similarity pressure distribution perpendicular

to the wall, ξ is the dimensionless wall distance, p_0 is pressure at surface of the disk, and p is the pressure distribution function. Equations (1)–(4) can be transformed into the following ordinary differential equation system [20,24,54]:

$$2F(\xi) + \frac{\mathrm{d}}{\mathrm{d}\xi}H(\xi) = 0 \tag{7}$$

$$F(\xi)^2 + \frac{\mathrm{d}}{\mathrm{d}\xi}F(\xi)H(\xi) - G(\xi)^2 - \frac{\mathrm{d}^2}{\mathrm{d}\xi^2}F(\xi) = 0 \tag{8}$$

$$2F(\xi)G(\xi) + H(\xi)\frac{\mathrm{d}}{\mathrm{d}\xi}G(\xi) - \frac{\mathrm{d}^2}{\mathrm{d}\xi^2}G(\xi) = 0 \tag{9}$$

$$\frac{\mathrm{d}}{\mathrm{d}\xi}P(\xi) + H(\xi)\frac{\mathrm{d}}{\mathrm{d}\xi}H(\xi) - \frac{\mathrm{d}^2}{\mathrm{d}\xi^2}H(\xi) = 0 \tag{10}$$

The boundary conditions of Equation (5) are reduced to the following dimensionless form by using Von Kármán similarity transformation variables [20,24,54]:

$$\begin{aligned} F(0) = 0, G(0) = 1, H(0) = 0, \\ P(0) = 0, F(\infty) = 0, G(\infty) = 0. \end{aligned} \tag{11}$$

According to the Equations (7)–(10), the velocity fields of $F(\xi)$, $H(\xi)$, and $G(\xi)$ are coupled with each other except for the $P(\xi)$ and the pressure distribution perpendicular to the wall can be determined after solving Equations (7)–(9) with their corresponding boundary conditions of Equation (11). First the velocity field is determined from solving the Equations (7)–(10), and then the $P(\xi)$ is calculated. So, the pressure can be found as below [54]:

$$P(\xi) = \int \frac{\mathrm{d}}{\mathrm{d}\xi}P(\xi)\mathrm{d}\xi = \int \left[\frac{\mathrm{d}^2}{\mathrm{d}\xi^2}H(\xi) - H(\xi)\frac{\mathrm{d}}{\mathrm{d}\xi}H(\xi)\right]\mathrm{d}\xi = \frac{\mathrm{d}}{\mathrm{d}\xi}H(\xi) - \frac{1}{2}H(\xi)^2 \tag{12}$$

In addition to obtaining the solution of the pressure distribution after solving Equations (7)–(9), it is possible to obtain the thickness of the layer, the slope of the streamlines at the wall to the circumferential direction, the peripheral component of the shear stress of the wall, the moment of one side of the wetted disk, the dimensionless coefficient for the moment on both sides of the wetted disk, the Reynolds number in terms of the finite radius of the disk, the volume flux, and the mechanical power [54].

By substituting a specific value of $\xi = \xi_{1\%}$ into Equation (13) when the fluid's circumferential velocity of V_r is approximately 1% of the disk velocity, the layer thickness of δ can be calculated as below:

$$\delta = \xi(\nu/\Omega)^{1/2} \tag{13}$$

The slope of the flow lines in the wall in the circumferential direction is denoted by φ_0 and it is formulated as below:

$$\varphi_0 = \tan^{-1}\left(\left(-\frac{\partial V_r/\partial z}{\partial V_\theta/\partial z}\right)_w\right) = \tan^{-1}\left(-\frac{F'(0)}{G'(0)}\right) \tag{14}$$

The parameters of δ and φ_0 are related only to rotating disks with infinite radius. The results now apply to a circular disk of finite radius R. It is certainly allowed if the radius R is large compared to the thickness δ of the disc carrier layer so that the edge effects are limited in the entire circular region. into a small ring-shaped area. The circumferential component of the wall shear stress is denoted by $\tau_{z\varphi}$ and it is as below:

$$\tau_{z\varphi} = \mu(\partial V_\theta/\partial z)_w = \rho r\Omega(\nu\Omega)^{1/2}G'(0) \tag{15}$$

The moment of a disk wetted on one side is denoted by M and it is as follows:

$$M = \int_0^R -2\pi r^2\tau_{z\phi}\mathrm{d}r = -\frac{\pi}{2}\rho R^4(\nu\Omega^3)^{\frac{1}{2}}G'(0) \tag{16}$$

where r is variable of radius and R is the finite radius of the disk. It is common to have the following dimensionless coefficient of c_M for the moment introduced for the disc wetted on both sides:

$$c_M = \frac{2M}{\rho\Omega^2(R^5/2)} \tag{17}$$

The Reynolds number of Re is formulated as below:

$$Re = \frac{R^2\Omega}{\nu} \tag{18}$$

Due to considering the laminarity for the flow, the Reynolds number Equation (18) is valid up to 3×10^5 [54]. The parameters of $\tau_{z\phi}$, M, c_M, and Re that are already mentioned in Equations (15)–(18) can be calculated only when the radius of the disk is finite.

The volume flux that is sucked in the axial direction towards the plate and injected radially out by the centrifugal force from around a disk with a finite radius of R, is calculated as follows [54]:

$$Q = 2\pi R\int_0^\infty V_r\mathrm{d}z = -H(\infty)\pi R^2(\nu\Omega)^{\frac{1}{2}} \tag{19}$$

where ∞ is the maximum value of ξ that is possible to calculate. Considering the proportionality of the pressure difference on the disc with $\rho\nu\Omega$, it can be said that at low viscosities, the pressure difference is very small, and the pressure depends only on the axial distance from the wall and therefore is independent of the radius R [54]. Since the fluid flow through the rotating discs acts as a pump, the fluid flow also experiences an increase in mechanical power P_M due to the increase in total pressure and is calculated as follows [54]:

$$P_M = \int_0^\infty \left[p + \frac{\rho}{2}\left(V_r^2 + V_\theta^2 + V_z^2\right)\right] 2\pi R V_r\mathrm{d}z = \pi\rho R^4\Omega(\nu/\Omega)^{1/2}\left[\int_0^\infty (F(\xi)^2 + G(\xi)^2)F(\xi)\mathrm{d}\xi - \frac{4}{Re}\int_0^\infty F(\xi)^2\mathrm{d}\xi\right] \tag{20}$$

Calculation of P_M is possible only when exact solutions of Equations (7)–(9) are obtained.

3. Mathematical description

3.1. Description of the HAN method

A new semi-analytical method called the HAN method [38,44,45,48] is capable of approximating many problems with unsolvable nonlinear equations. In this mathematical method for finding the analytical solution of an equation, the equation must first be solved numerically, and the numerical method in this method is not limited to a specific method, and this flexibility is one of the strengths of this method. Another strength of the HAN method is that it can be a power series with a much more limited number of sentences than other semi-analytical solutions. The explanation of this method is as follows:

The general form of differential equations with order of m will be as follows:

$$\Gamma\left(f(\xi), f'(\xi), f''(\xi), \dots, f^{(m)}(\xi)\right) = 0 \tag{21}$$

Equation (21) represents a nonlinear differential equation where Γ is a function of $f(\xi)$. The function $f(\xi)$ and its derivatives with respect to ξ are displayed as follows:

$$\begin{cases} f(\xi) = f_0, & f'(\xi) = f_1, \dots, & f^{(m-1)}(\xi) = f_{m-1} \text{ when } \xi = 0 \\ f(\xi) = f_{L_0}, & f'(\xi) = f_{L_1}, \dots, & f^{(m-1)}(\xi) = f_{L_{m-1}} \text{ when } \xi = L \end{cases} \tag{22}$$

The following n-order polynomial with constant coefficients is considered as the solution of Equation (21):

$$f(\xi) = \sum_{i=0}^{n} a_i \xi^i = a_0 + a_1\xi^1 + a_2\xi^2 + \cdots + a_n\xi^n \tag{23}$$

The solution of Equation (21) is Equation (23), which is an nth-order polynomial with $n + 1$ unknown coefficients. Solving a system of $n + 1$ unknowns and $n + 1$ equations can determine unknown coefficients of Equation (23), or in other words, the solution of Equation (21) is calculated. We can achieve some of these equations with boundary conditions of the problem, which is shown in the following Equations (24) and (25):

$$\begin{cases} f(0) = a_0 = f_0, \\ f'(0) = a_1 = f_1, \\ f''(0) = a_2 = f_2, \\ \quad . \quad . \quad . \\ \quad . \quad . \quad . \end{cases} \tag{24}$$

$$\begin{cases} f(L) = a_0 + a_1L + a_2L^2 + \cdots + a_nL^n = f_{L_0} \\ f'(L) = a_1 + 2a_2L + 3a_3L^2 + \cdots + na_nL^{n-1} = f_{L_1} \\ f''(L) = 2a_2 + 6a_3L + 12a_4L^2 + \cdots + n(n-1)a_nL^{n-2} = f_{L_2} \\ \qquad\qquad\qquad\qquad\quad . \quad . \quad . \\ \qquad\qquad\qquad\qquad\quad . \quad . \quad . \end{cases} \tag{25}$$

According to the numerical solution of Equation (21), the new approximated boundary conditions are as follows:

The constructed equations from boundary conditions of the problem, as they can be seen in Equations (24) and (25), are limited because we assume the value of n is higher than m earlier in this methodology. All the explanations given about HAN from Equations (21)–(25) overlap with the AGM method, but from here on the difference between the HAN and AGM methods will be explained. To increase the number of constructed equations to $n + 1$ equations, more boundary equations are needed, and the numerical methods (no matter which numerical method) can approximate these additional boundary conditions for making the remaining needed equations. So, the new approximated boundary conditions are as follows:

$$\begin{cases} f(\xi) = \alpha_0, f'(\xi) = \alpha_1, \dots, f^{(m-1)}(\xi) = \alpha_{m-1} \; at \; \xi = L_0 \\ f(\xi) = \beta_0, f'(\xi) = \beta_1, \dots, f^{(m-1)}(\xi) = \beta_{m-1} \; at \; \xi = L_1 \\ f(\xi) = \gamma_0, f'(\xi) = \gamma_1, \dots, f^{(m-1)}(\xi) = \gamma_{m-1} \; at \; \xi = L_2 \\ \qquad\qquad . \qquad . \qquad . \\ \qquad\qquad . \qquad . \qquad . \\ f(\xi) = \varepsilon_0, f'(\xi) = \varepsilon_1, \dots, f^{(m-1)}(\xi) = \varepsilon_{m-1} \; at \; \xi = L_z \end{cases} \tag{26}$$

The new approximated boundary conditions of Equation (26) from the numerical results can be used like Equations (24) and (25) for making new equations, and from Equation (26) it can be derived as many equations as are needed to create a system with $n + 1$ equations and $n + 1$ unknowns. For instance, from the following equations, Equations (27)–(30) shown new equations in addition to equations that were made through the boundary conditions of the problem:

$$\begin{cases} f(L_0) = a_0 + a_1(L_0) + a_2(L_0)^2 + \cdots + a_n(L_0)^n = \alpha_0, \\ f'(L_0) = a_1 + 2a_2(L_0) + 3a_3(L_0)^2 + \cdots + na_n(L_0)^{n-1} = \alpha_1, \\ f''(L_0) = 2a_2 + 6a_3(L_0) + 12a_4(L_0)^2 + \cdots + n(n-1)a_n(L_0)^{n-2} = \alpha_2, \\ \qquad\qquad . \qquad . \qquad . \\ \qquad\qquad . \qquad . \qquad . \\ \left(f^{(m-1)}(\xi)\right)_{\xi=L_0} = \alpha_{m-1}. \end{cases} \tag{27}$$

$$\begin{cases} f(L_1) = a_0 + a_1(L_1) + a_2(L_1)^2 + \cdots + a_n(L_1)^n = \beta_0, \\ f'(L_1) = a_1 + 2a_2(L_1) + 3a_3(L_1)^2 + \cdots + na_n(L_1)^{n-1} = \beta_1, \\ f''(L_1) = 2a_2 + 6a_3(L_1) + 12a_4(L_1)^2 + \cdots + n(n-1)a_n(L_1)^{n-2} = \beta_2, \\ \qquad\qquad . \qquad . \qquad . \\ \qquad\qquad . \qquad . \qquad . \\ \left(f^{(m-1)}(\xi)\right)_{\xi=L_1} = \beta_{m-1}. \end{cases} \tag{28}$$

$$\begin{cases} f(L_2) = a_0 + a_1(L_2) + a_2(L_2)^2 + \cdots + a_n(L_2)^n = \gamma_0, \\ f'(L_2) = a_1 + 2a_2(L_2) + 3a_3(L_2)^2 + \cdots + na_n(L_2)^{n-1} = \gamma_1, \\ f''(L_2) = 2a_2 + 6a_3(L_2) + 12a_4(L_2)^2 + \cdots + n(n-1)a_n(L_2)^{n-2} = \gamma_2, \\ \qquad\qquad . \qquad . \qquad . \\ \qquad\qquad . \qquad . \qquad . \\ \left(f^{(m-1)}(\xi)\right)_{\xi=L_2} = \gamma_{m-1}. \end{cases} \tag{29}$$

$$\begin{cases} f(L_z) = a_0 + a_1(L_z) + a_2(L_z)^2 + \cdots + a_n(L_z)^n = \varepsilon_0, \\ f'(L_z) = a_1 + 2a_2(L_z) + 3a_3(L_z)^2 + \cdots + na_n(L_z)^{n-1} = \varepsilon_1, \\ f''(L_z) = 2a_2 + 6a_3(L_z) + 12a_4(L_z)^2 + \cdots + n(n-1)a_n(L_z)^{n-2} = \varepsilon_2, \\ \qquad\qquad \vdots \qquad \vdots \qquad \vdots \\ \left(f^{(m-1)}(\xi)\right)_{\xi=L_z} = \varepsilon_{m-1}. \end{cases} \tag{30}$$

By solving the system of $n + 1$ equations with $n + 1$ unknowns that we already constructed, the constant coefficients of the polynomial solution of Equation (23) can be determined, and then these obtained values can be used as a semi-analytical solution for Equation (21). As mentioned earlier in this section of the article, it should be considered that only a limited part of the AGM method overlaps with the HAN method, and these two methods are completely different.

3.2. Application of the HAN-method

This section is about showing the application of the HAN method in finding the analytical solution of the Von Kármán equations. The governing equations of Von Kármán and their corresponding boundary conditions of Equations (7)–(11) were mentioned in Sec. (2) of the current paper. So, according to explanations given in Sec. (3.1), it is assumed that the following series are the solutions of Equations (7)–(9):

$$F(\xi) = \sum_{i=0}^{10} a_i \xi^i \, , G(\xi) = \sum_{i=0}^{10} b_i \xi^i \, , H(\xi) = \sum_{i=0}^{10} c_i \xi^i . \tag{31}$$

There are 33 unknown coefficients in Equation (31), and there have to be 33 equations in order to determine these series solutions of Equations (7)–(9). According to Equation (11), some limited number of equations can be made by the boundary conditions of the problem as below:

$$F(\xi)|_{\xi=0} = \sum_{i=0}^{9} a_i \xi^i \Big|_{\xi=0} = a_0 = 0 \tag{32}$$

$$G(\xi)|_{\xi=0} = \sum_{i=0}^{9} b_i \xi^i \Big|_{\xi=0} = b_0 = 1 \tag{33}$$

$$H(\xi)|_{\xi=0} = \sum_{i=0}^{9} c_i \xi^i \Big|_{\xi=0} = c_0 = 0 \tag{34}$$

$$F(\xi)|_{\xi=+\infty} = \sum_{i=0}^{9} a_i \xi^i \Big|_{\xi=+\infty} = 0 \tag{35}$$

$$G(\xi)|_{\xi=+\infty} = \sum_{i=0}^{9} b_i \xi^i \Big|_{\xi=+\infty} = 0 \tag{36}$$

where the Equations (32)–(36) are 5 equations, but due to the semi-infinity of the boundary conditions of the problem, it is not possible to determine what ξ is at infinity. Then, among Equations (32)–(36), only Equations (32)–(34) are applicable. So, it is obvious that 3 equations are not enough because 30 more equations are needed to find all the unknown coefficients. The remaining equations must be made by the new boundary conditions, and it is possible when they are approximated by a numerical method of RK4. So, by solving Equations (7)–(9) with boundary conditions of Equations (11) numerically, the following approximated boundary conditions can be calculated, and they are demonstrated in the following **Table 1**:

Table 1. The numerical results $F(\xi)$, $G(\xi)$, $H(\xi)$, and $P(\xi)$ from RK4 method.

The Runge-Kutta solutions					
ξ	$F(\xi)$	$F'(\xi)$	$G(\xi)$	$G'(\xi)$	$H(\xi)$
0	0	0.5101887308	1	−0.6158937994	0
1	0.1801057123	−0.0157626785	0.4766431672	−0.3911422046	−0.2654256959
2	0.1187359055	−0.0739557439	0.2033285370	−0.1771959836	−0.5729889369
3	0.0579431177	−0.0455178756	0.0844172286	−0.0746402952	−0.7447389737
4	0.0254429777	−0.0216794352	0.0347439986	−0.0309804734	−0.8241490046
5	0.0106359117	−0.0094759338	0.0141547055	−0.0128296650	−0.8582098557
6	0.0042708523	−0.0040080425	0.0056284748	−0.0053135787	−0.8722151508
7	0.0015961207	−0.0016735748	0.0020965052	−0.0022017798	−0.8776977020
8	0.0004820674	−0.0006953943	0.0006326466	−0.0009128045	−0.8796148863
9	0.0000195560	−0.0002884880	0.0000256624	−0.0003785633	−0.8800495476
9.069895	0	−0.0002712777	0		−0.8800509002

The remaining 30 equations can be made from the approximated boundary conditions of **Table 1** just like how Equations (32)–(36) are created from Equation (11). Considering that writing these 30 new equations makes the paper longer and they are like Equations (32)–(36), writing them is omitted. Having 3 equations that were made from the boundary conditions of the problem and 30 other equations that were obtained from the approximated boundary conditions of **Table 1** made a mathematical system of 33 equations and 33 unknowns, and by solving it, all the unknown coefficients of Equation (31) are determined. So, the analytical solutions of Equations (7)–(10) are as follows:

$$\begin{aligned} F(\xi) = {} & -6.07431182 \times 10^{-9}\xi^{10} + 3.90124387 \times 10^{-7}\xi^{9} \\ & - 0.00001118416228\xi^{8} + 0.000188446481\xi^{7} \\ & - 0.00206538565\xi^{6} + 0.01535505061\xi\text{^}5 \\ & - 0.0779872538\xi\text{^}4 + 0.2632321130\xi\text{^}3 \\ & - 0.5413702437\xi\text{^}2 + 0.5227637854\xi, \end{aligned} \tag{37}$$

$$\begin{aligned} G(\xi) = & -1.77745633 \times 10^{-8}\xi^{10} + 9.75590571 \times 10^{-7}\xi^{9} \\ & - 0.00001118416228\xi^{8} + 0.000188446481\xi^{7} \\ & - 0.00206538565\xi^{6} + 0.01535505061\xi^{5} \\ & - 0.0779872538\xi^{4} + 0.2632321130\xi^{3} - 0.5413702437\xi^{2} \\ & + 0.5227637854\xi, \end{aligned} \tag{38}$$

$$\begin{aligned} H(\xi) = & -1.97842177 \times 10^{-8}\xi^{10} + 1.150613857 \times 10^{-6}\xi^{9} \\ & - 0.0000296999488\xi^{8} + 0.000448000973\xi^{7} \\ & - 0.00436837101\xi^{6} + 0.0286496680\xi^{5} - 0.1263248188\xi^{4} \\ & + 0.3550648993\xi^{3} - 0.5210507216\xi^{2} + 0.0021842162\xi. \end{aligned} \tag{39}$$

where Equation (37) represents the similarity radial velocity, Equation (38) represents the similarity azimuthal velocity field, and Equation (39) represents the similarity axial velocity field. According to Equation (12) in Sec. (2), the pressure field of $P(\xi)$ can be determined from the analytical solution of the axial velocity field of Equation (39). So, the pressure fields of $P(\xi)$ is as follows:

$$\begin{aligned} P(\xi) = & -1.042101443x + 1.065192313x^{2} - 0.5041611878x^{3} \\ & + 0.0067258742x^{4} + 0.1590725166x^{5} - 0.1257837496x^{6} \\ & + 0.05955338116x^{7} - 0.02041823728x^{8} \\ & + 0.005403517588x^{9} - 0.001136782528x^{10} \\ & - 1.957076350 \times 10^{-16}x^{20} + 2.276399504 \times 10^{-14}x^{19} \\ & - 1.249546377 \times 10^{-12}x^{18} + 4.303652142 \times 10^{-11}x^{17} \\ & - 1.042944410 \times 10^{-9}x^{16} + 1.889872545 \times 10^{-8}x^{15} \\ & - 2.655567739 \times 10^{-7}x^{14} + 2.960303904 \times 10^{-6}x^{13} \\ & - 0.00002654710360x^{12} + 0.0001928910016x^{11} \\ & + 0.0021842162, \end{aligned} \tag{40}$$

where Equations (37)–(40) are valid when $0 \leq \xi \leq 9$ and Reynolds numbers are up to 3×10^{5}. The graphical representation of Equations (37)–(40) is shown in **Figures 2** and **3** as below:

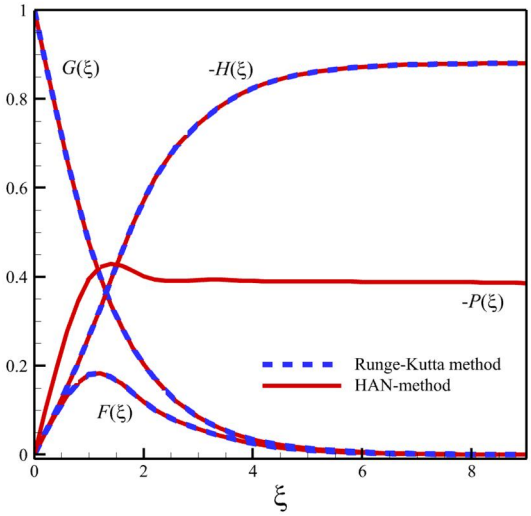

Figure 2. The graphical representation of $F(\xi)$, $G(\xi)$, $-H(\xi)$, and $-P(\xi)$ from the HAN method when they were compared with the RK4 solution.

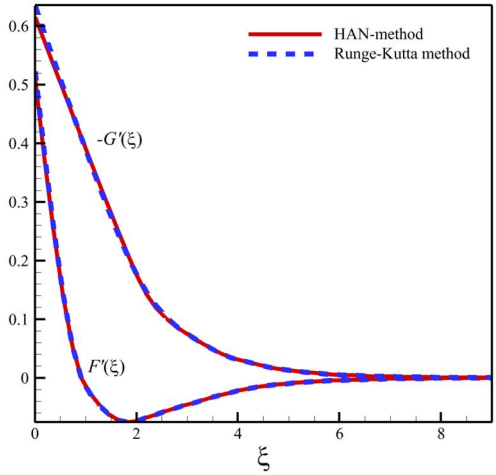

Figure 3. The graphical representation of $F'(\xi)$ and $-G'(\xi)$ from the HAN method when they were compared with the RK4 solution.

Considering the results of the analytical solutions of Equations (37)–(40) were made with the help of Equation (11) and the approximated boundary conditions of **Table 1**, it should be proved that they are the solutions of Equations (7)–(10). So, by substituting $F(\xi)$, $G(\xi)$, and $H(\xi)$ in Equations (7)–(9), the following functions Eq_1, Eq_2, and Eq_3 are concluded as below:

$$\begin{aligned} Eq_1(\xi) &:= 2F(\xi) + \frac{d}{d\xi}H(\xi) \\ &= -0.000012012799 85\xi^8 + 0.0001392933716\xi^7 \\ &- 0.000994764489\xi^6 + 0.00449987516\xi^5 \\ &- 0.017545789\,\xi^2 - 0.0127261676\xi^4 + 0.0211649508\xi^3 \\ &+ 0.003426128\xi + 0.0021842162, \end{aligned} \tag{41}$$

$$\begin{aligned} Eq_2(\xi) &:= F(\xi)^2 + \frac{d}{d\xi}F(\xi)H(\xi) - G(\xi)^2 - \frac{d^2}{d\xi^2}F(\xi) \\ &= -0.307402949\xi + 0.4107046877\xi^2 - 0.2321553404\xi^3 \\ &- 0.00843845310\xi^4 + 0.1086421640\xi^5 \\ &- 0.09009491674\xi^6 + 0.04492264842\xi^7 \\ &- 0.01617323018\xi^8 + 0.004491785456\xi^9 \\ &- 0.0009928055786\xi^{10} - 2.790378364 \times 10^{-16}\xi^{20} \\ &+ 3.114367344 \times 10^{-14}\xi^{19} - 1.636267524 \times 10^{-12}\xi^{18} \\ &+ 5.381185038 \times 10^{-11}\xi^{17} - 1.242466579 \times 10^{-9}\xi^{16} \\ &+ 2.141012685 \times 10^{-8}\xi^{15} - 2.856808912 \times 10^{-7}\xi^{14} \\ &+ 3.021499866 \times 10^{-6}\xi^{13} - 0.00002570345111\xi^{12} \\ &+ 0.0001772650607\xi^{11} + 0.082740487, \end{aligned} \tag{42}$$

$$
\begin{aligned}
Eq_3(\xi) \coloneqq\ & 2F(\xi)G(\xi) + H(\xi)\frac{d}{d\xi}G(\xi) - \frac{d^2}{d\xi^2}G(\xi) \\
&= 0.4839414608\xi - 0.7624858733\xi^2 + 0.6759490582\xi^3 \\
&- 0.3973164381\xi^4 + 0.1695434802\xi^5 - 0.05457796061\xi^6 \\
&+ 0.01297296166\xi^7 - 0.001964958929\xi^8 \\
&+ 0.000027790893\xi^9 + 0.000086658628\xi^{10} \\
&+ 2.159364798 \times 10^{-16}\xi^{20} - 2.220410560 \times 10^{-14}\xi^{19} \\
&+ 1.065302664 \times 10^{-12}\xi^{18} - 3.164126757 \times 10^{-11}\xi^{17} \\
&+ 6.505497573 \times 10^{-10}\xi^{16} - 9.79783102 \times 10^{-9}\xi^{15} \\
&+ 1.113614153 \times 10^{-7}\xi^{14} - 9.66164830 \times 10^{-7}\xi^{13} \\
&+ 6.34572864 \times 10^{-6}\xi^{12} - 0.0000301523536\xi^{11} \\
&- 0.1199093502.
\end{aligned}
\tag{43}
$$

By plotting the functions $Eq_1(\xi)$, $Eq_2(\xi)$, and $Eq_3(\xi)$ in the following figure, when $0 \leq \xi \leq 9$, the local error value of the obtained analytical solutions can be calculated as follows:

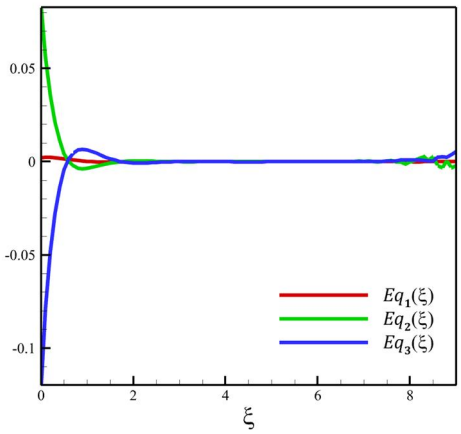

Figure 4. The graphical representation of $Eq_1(\xi)$, $Eq_2(\xi)$, and $Eq_3(\xi)$, when the HAN solutions were substituted in the governing equations.

As the error rate of the HAN solution can be seen in **Figure 4**, the maximum positive error of the semi-analytical solutions of Equations (7)–(9) is equal to 0.082740487, and the maximum negative error is equal to −0.1199093502.

4. Validation

Considering that the Von Kármán equations are not solved for the first time, it is necessary to compare them with previously published solutions. In **Figures 5–10**, the analytical results of HAN are compared with the numerical results of Von Kármán [2] and Cochran [3] as follows:

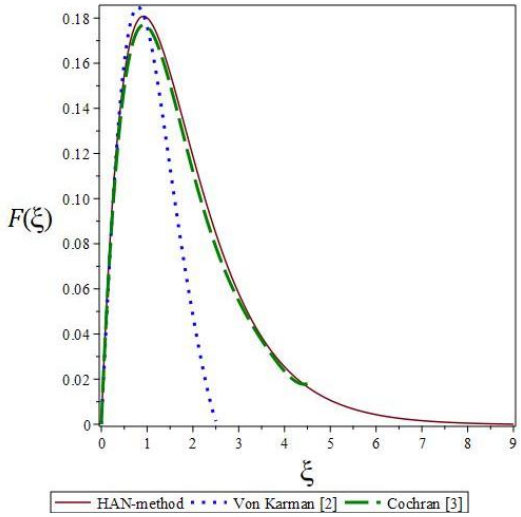

Figure 5. The graphical representation of $F(\xi)$ from the HAN method when they were compared with Von Kármán and Cochran results.

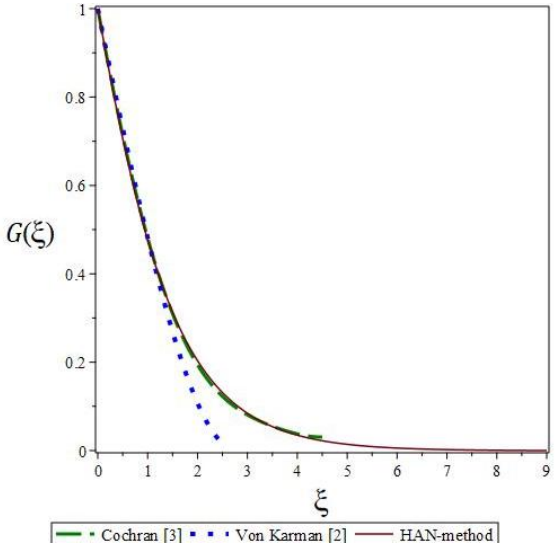

Figure 6. The graphical representation of $G(\xi)$ from the HAN method when they were compared with Von Kármán and Cochran results.

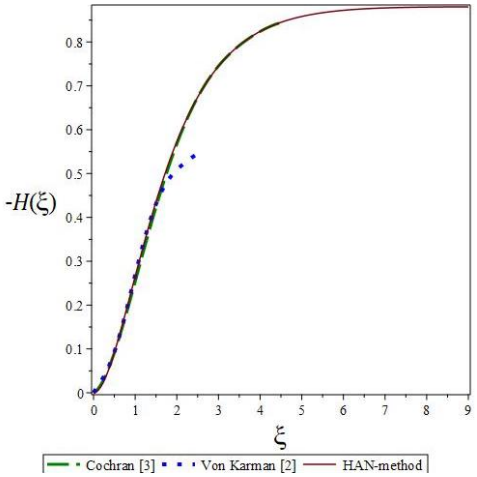

Figure 7. The graphical representation of $-H(\xi)$ from the HAN method when they were compared with Von Kármán and Cochran results.

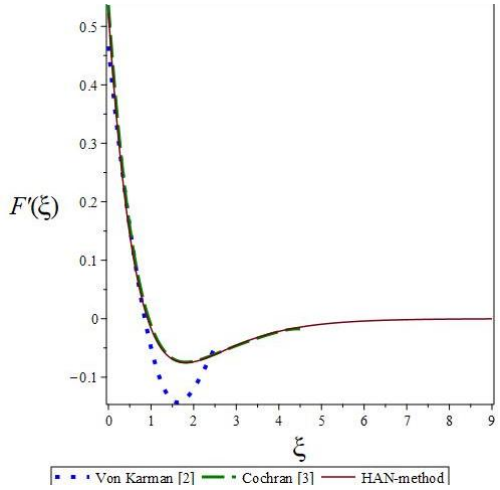

Figure 8. The graphical representation of $F'(\xi)$ from the HAN method when they were compared with Von Kármán and Cochran results.

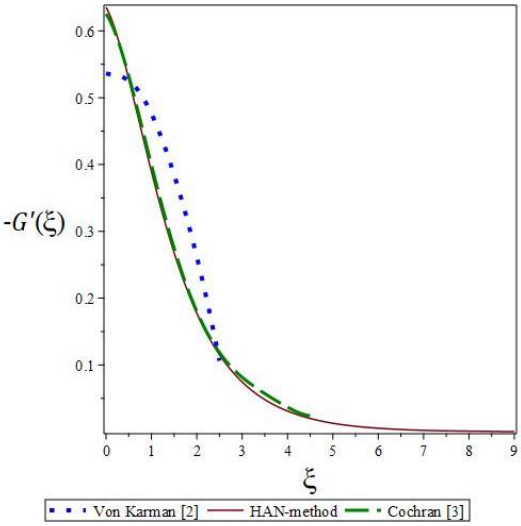

Figure 9. The graphical representation of $-G'(\xi)$ from the HAN method when they were compared with Von Kármán and Cochran results.

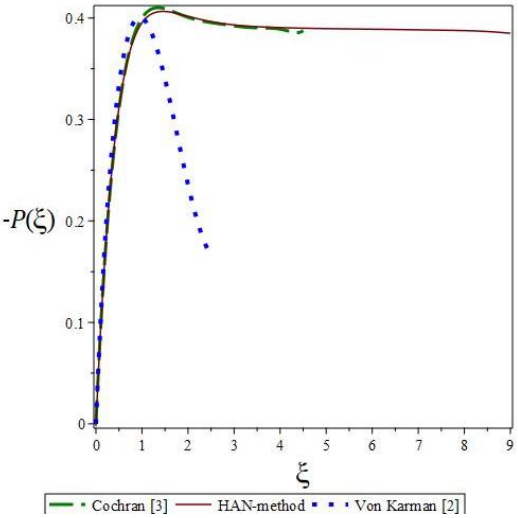

Figure 10. The graphical representation of $-P(\xi)$ from the HAN method when they were compared with Von Kármán and Cochran results.

The reason for the superiority of HAN solutions over previous numerical solutions can be seen in **Figures 5–10**. According to **Figures 2** and **3**, the analytical solutions (37–39) are very close to the Runge-Kutta numerical solution because the analytical solutions of HAN are constructed from the numerical solution. The validity of the results obtained from the numerical methods and especially the Runge-Kutta method in this research can be expressed in this way: The analytical solution of HAN can be placed in the differential equations, and its accuracy can be seen in **Figure 4**. According to **Figure 4**, the accuracy of solving the rotating Von Kármán fluid problem exceeds the minimum engineering value, which means that these solutions can be used for other applications that have an accuracy beyond engineering problems.

5. Results and discussion

According to the second part of the article, which is related to the research methodology, it is possible to obtain many practical outputs from the analytical solutions of Equations (7)–(9) by using the HAN method. Despite this classic Von Kármán problem about the rotation of a disk, which is one of the basic problems in fluid mechanics and boundary layer theory, it has solutions that are not very acceptable in the diagnosis and results of the previous solutions. Considering that the obtained analytical solutions have sufficient accuracy, these solutions can be used to obtain more accurate physical results. Considering that the Equations (37)–(39) are the analytical solution of the system of differential Equations (7) and (8), in addition to **Table 2**, the thickness of the layer of δ, the slope of the streamlines at the wall to the circumferential direction of φ_0, the peripheral component of the shear stress of the wall $\tau_{z\varphi}$, the moment of one side of the wetted disk M, the dimensionless coefficient for the moment on both sides of the wetted disk c_M, the volume flux of Q, and the mechanical power of P_M can be calculated. **Table 2** is as follows:

Table 2. The analytical results $F(\xi)$, $G(\xi)$, $H(\xi)$, and $P(\xi)$ from HAN-method.

The HAN solutions					
ξ	$F(\xi)$	$F'(\xi)$	$G(\xi)$	$G'(\xi)$	$H(\xi)$
0	0	0.5227637854	1	−0.6354239499	0
1	0.1801057122	−0.0166133362	0.4766431674	−0.3894695277	−0.2654256961
2	0.118735904	−0.0738347626	0.2033285374	−0.1775066595	−0.5729889366
3	0.057943116	−0.0455456786	0.0844172287	−0.0745436673	−0.7447389684
4	0.025442973	−0.0216700926	0.034744002	−0.0310263911	−0.8241490012
5	0.010635897	−0.0094802696	0.014154687	−0.0127978089	−0.8582098690
6	0.004270832	−0.0040054766	0.005628444	−0.0053453487	−0.8722151328
7	0.001596018	−0.0016753136	0.002096310	−0.0021575985	−0.8776977466
8	0.000481883	−0.0006952106	0.000632846	−0.0009940183	−0.8796148504
9	0.000019629	−0.0002928376	0.000025802	−0.0003436079	−0.8800500042

The thickness of the boundary layer that was formed on the infinite radius disk ends when the circumferential velocity of the fluid reaches 1% of the disk's velocity. Since the circumferential velocity of fluid is V_r and is proportional with $F(\xi)$, a

specific value of $\xi = \xi_{1\%}$ must be found when $F(\xi) = 0.01$. So, the value of $\xi_{1\%}$ can be determined by interpolating in **Table 1**, and according to Equation (13), the thickness of the boundary layer of δ, that was formed on the disk can be calculated as below:

$$\delta = \xi_{1\%}(\nu/\Omega)^{1/2} = 5.099904243(\nu/\Omega)^{1/2} \tag{44}$$

According to Schlichting and Gersten [54], the value of $\xi_{1\%}$ was calculated as 5.5 before, but Equation (44) was stated more accurately. According to Equation (14), the slope of the flow lines in the wall in the circumferential direction can be calculated as below:

$$\varphi_0 = tan^{-1}\left(-\frac{F'(0)}{G'(0)}\right) = tan^{-1}\left(-\frac{0.5227637854}{-0.6354239499}\right) \approx 39.444° \tag{45}$$

where φ_0 was calculated 39.6° before [54], but Equation (45) gives a more accurate result. So, in **Figure 1**, the value of φ_0 is 39.444°. According to Equation (15), the circumferential component of the wall shear stress can be calculated as follows:

$$\tau_{z\varphi} = \rho r\Omega(\nu\Omega)^{1/2}G'(0) = -0.6354239499\rho r\Omega(\nu\Omega)^{\frac{1}{2}} \tag{46}$$

The moment of a disk wetted on one side, according to Equation (16), can be determined as follows:

$$M = -\frac{\pi}{2}\rho R^4(\nu\Omega^3)^{\frac{1}{2}}G'(0) = 0.9981216066\rho R^4(\nu\Omega^3)^{\frac{1}{2}} \tag{47}$$

The moment for disc wetting on both sides, according to Equation (17), can be found as below:

$$c_M = \frac{2M}{\rho\Omega^2(R^5/2)} = 1.996243213\frac{R^4(\nu\Omega^3)^{\frac{1}{2}}}{\Omega^2(R^5/2)} \tag{48}$$

The value of $G'(0)$ was calculated as −0.61592 before [54], but Equations (46)–(48) give more accurate results. According to Equation (19), the volume flux can be calculated as below:

$$Q = -H(\infty)\pi R^2(\nu\Omega)^{\frac{1}{2}} = 0.8800500042\pi R^2(\nu\Omega)^{\frac{1}{2}} \tag{49}$$

where $H(\infty)$ was equals to 0.88446 according to Schlichting and Gersten [54], but Equation (49) calculates the volume flux more accurately. According to Equation (20), the mechanical power of P_M calculated as follows:

$$P_M = \pi\rho R^4\Omega(\nu/\Omega)^{1/2}\left[\int_0^\infty (F(\xi)^2 + G(\xi)^2)F(\xi)d\xi - \frac{4}{Re}\int_0^\infty F(\xi)^2 d\xi\right] \tag{50}$$

With considering $\xi = 9$ instead of ∞ and by substituting Equations (37) and (38) in Equation (50), the mechanical power can be determined as follows:

$$P_M = \left(0.08823081036 - \frac{0.2166429892}{Re}\right)\pi\rho R^4\Omega(\nu/\Omega)^{1/2} \tag{51}$$

Considering large Reynolds numbers, Equation (51) reduces to the following form:

$$P_M = (0.08823081036)\pi\rho R^4\Omega(\nu/\Omega)^{1/2} \quad (52)$$

where Equation (52) is approximately like the previous calculations and states the accuracy of Equations (37)–(39).

6. Conclusion

6.1. Summary of mathematical achievements

This study introduced the Hybrid Analytical and Numerical (HAN) method as a novel approach for solving nonlinear fluid flow problems, emphasizing its accuracy and flexibility. The method's analytical solutions were derived from numerical results obtained using the Runge-Kutta method, as depicted in **Figures 2** and **3**. The numerical solution, shown as a blue dashed line, served as the foundation for constructing the analytical solution, illustrated by the solid red line in the same figures. Importantly, **Figure 4** does not represent numerical errors but rather demonstrates the correctness of the semi-analytical solution derived through the HAN method, based on the substitution of Equations (37)–(39) into the original differential equations such as Equations (7)–(9). Comparisons with [2,3] validate the higher accuracy of the HAN method. The claim that the HAN method offers improved accuracy is further substantiated by **Figures 5–10**. While the method theoretically allows for an unlimited number of polynomial coefficients, practical considerations impose constraints. Increasing the number of terms in the polynomial solution can lead to significant errors rather than improving the results. In this study, 11 terms were selected as the optimal number to ensure accuracy, as outlined in Equation (31). This choice is supported by the high-quality results presented in the study, which demonstrate significant improvements over previous research. Increasing the number of terms beyond this limit would reduce the range of functions such as Equations (41)–(43) and diminish the solution's reliability, as reflected in **Figure 4**. The comparison between **Tables 1** and **2** underscores the validity of the HAN method. **Table 1** presents the numerical solution of Equations (7)–(9) derived via the Runge-Kutta method with the help of Maple mathematical software, renowned for its precision in solving nonlinear coupled differential equations. **Table 2** represents the analytical solution obtained using the HAN method, constructed from the numerical data in **Table 1**. The consistency between the two tables reaffirms the reliability and robustness of the HAN method's semi-analytical solutions, confirming their validity in addressing complex problems. The analysis of **Figure 4**, along with comparisons to the numerical solutions and prior research, highlights the advantages of the HAN method in capturing intricate details of nonlinear fluid flow phenomena. While some regions, such as those close to the disk surface or the edge of the boundary layer, exhibit noticeable discrepancies, these do not undermine the overall accuracy and reliability of the method. Instead, they showcase the method's potential for refining and extending analytical solutions for nonlinear problems. In conclusion, the HAN method offers a robust framework for solving nonlinear differential equations, combining the strengths of numerical and analytical approaches. Its effectiveness is demonstrated through comparisons with

prior studies, as well as the high accuracy of its results in addressing classical fluid flow problems. This research contributes significantly to both the theoretical and practical aspects of fluid mechanics, paving the way for further exploration and applications of hybrid methodologies in solving complex problems.

6.2. Summary of physical achievements

In this section, a summary of the achievements and novelty of this article is presented. The equations of this article were solved by the HAN mathematical method, not because they had not been solved yet, but because after all these years after the introduction of this problem, much more powerful calculation tools have been provided than before. At the same time, the equations of this article are simple, but they are very fundamental and practical, and any solution that is more accurate than the previous solutions can give more reliable results. The practicality of this classic problem is that the physics of this problem is like a three-dimensional pump, and, for example, if our solutions are accurate enough, they can be used even beyond engineering problems, such as medical problems. But another reason for writing the article is to show the application of the HAN method in non-linear problems, and even though the analytical solutions obtained from HAN are proven to be accurate, it is still possible to get much more accurate solutions from this method. Therefore, to finish the article, all the achievements of the article can be concluded as follows:

- The Hybrid Analytical and Numerical method (HAN method) is a powerful and flexible mathematical tool for solving nonlinear problems semi-analytically.
- The solutions of the Von Kármán equations for the rotation of a disk were approximated more accurately than before.
- Despite the application of the current solutions to a wide range of problems due to sufficient accuracy, it is still possible to obtain much more accurate solutions.
- The thickness of the boundary layer can be calculated more accurately with the help of the HAN method.
- If the slope of the flow lines in the wall in the circumferential direction is considered 39.444° instead of 39.6°, the results will be more accurate.
- More accurate results will be achieved by using current calculated parameters such as the circumferential component of the wall shear stress, the moment of a disk wetted on one side, and the moment for a disc wetted on both sides.
- The volume flux that is calculated in this study is more accurate than the previous ones.
- Unlike previous studies, the calculations of the mechanical power in this paper belong to different Reynolds numbers, and just for a special case when the Reynolds number is large, the calculations of the mechanical power are approximately the same as the previous ones.

While this study validates the accuracy of the HAN method through comparisons with [2,3], it is acknowledged that these references are somewhat dated. The selection of these comparisons aligns with the study's focus on solving the classical Von Kármán equations, ensuring consistency with the original formulation of the problem. Many recent studies utilize modified or extended versions of the Von Kármán equations, but the aim here has been to revisit the classical equations and improve the accuracy of

their solutions using the HAN method. As illustrated in **Figures 5–10**, the solutions derived in this study successfully demonstrate the precision of the HAN method. These comparisons with prior approximation methods highlight the validity and robustness of the presented approach in addressing this classical problem. By refining and extending existing results, this research underscores the novelty and significance of applying the HAN method to classical equations. Future studies could broaden the scope of comparisons to include newer approximation methods, particularly for modified versions of the equations, to further validate and enhance the persuasiveness of the HAN method's applications.

Conflict of interest: The author declares no conflict of interest.

References

1. Kataoka H, Tomiyama A, Hosokawa S, et al. Two-Phase Swirling Flow in a Gas-Liquid Separator. Journal of Power and Energy Systems. 2008; 2(4): 1120-1131. doi: 10.1299/jpes.2.1120
2. Kármán TV. About laminar and turbulent friction (German). ZAMM—Journal of Applied Mathematics and Mechanics. 1921; 1(4): 233-252. doi: 10.1002/zamm.19210010401
3. Cochran WG. The flow due to a rotating disc. Mathematical Proceedings of the Cambridge Philosophical Society. 1934; 30(3): 365-375. doi: 10.1017/s0305004100012561
4. Bödewadt UT. The rotary flow over solid ground (German). ZAMM—Journal of Applied Mathematics and Mechanics. 1940; 20(5): 241-253. doi: 10.1002/zamm.19400200502
5. Fettis HE. On the integration of a class of differential equations occurring in boundary layer and other hydrodynamic problems. In: Proceedings of the 4th Midwest Fluid Mechanics Conference; 1955.
6. Rogers MH, Lance GN. The rotationally symmetric flow of a viscous fluid in the presence of an infinite rotating disk. Journal of Fluid Mechanics. 1960; 7(4): 617-631. doi: 10.1017/s0022112060000335
7. Batchelor GK. Note on a class of solutions of the Navier-stokes equations representing steady rotationally-symmetric flow. The Quarterly Journal of Mechanics and Applied Mathematics. 1951; 4(1): 29-41. doi: 10.1093/qjmam/4.1.29
8. Benton ER. On the flow due to a rotating disk. Journal of Fluid Mechanics. 1966; 24(04): 781. doi: 10.1017/s0022112066001009
9. Zandbergen PJ, Dijkstra D. Von Karman Swirling Flows. Annual Review of Fluid Mechanics. 1987; 19(1): 465-491. doi: 10.1146/annurev.fl.19.010187.002341
10. Tien CL, Tsuji J. Heat transfer by laminar forced flow against a non-isothermal rotating disk. International Journal of Heat and Mass Transfer. 1964; 7(2): 247-252. doi: 10.1016/0017-9310(64)90089-4
11. Evans GH, Greif R. Forced flow near a heated rotating disk: a similarity solution. Numerical Heat Transfer. 1988; 14(3): 373-387. doi: 10.1080/10407788808913650
12. Sharma H. Flow of a second-order fluid between two infinite rotating discs with injection. International Journal of Mathematics Trends and Technology. 1975.
13. Kumari M, Takhar HS, Nath G. Nonaxisymmetric unsteady motion over a rotating disk in the presence of free convection and magnetic field. International journal of engineering science. 1993; 31(12): 1659-1668. doi: 10.1016/0020-7225(93)90081-5
14. Öztekin A, Brown RA. Instability of a viscoelastic fluid between rotating parallel disks: analysis for the Oldroyd-B fluid. Journal of Fluid Mechanics. 1993; 255(1): 473. doi: 10.1017/s0022112093002563
15. Deshpande AG, Ghosh SG. Numerical study of the unsteady flow in fluid-particle suspension from an infinite rotating disk. Indian Journal of Pure and Applied Mathematics. 1996.
16. Choudhury R, Das ALOK. Elastico-viscous flow and heat transfer between two rotating discs of different transpiration. Indian Journal of Pure and Applied Mathematics. 1997.
17. Shevchuk IV, Buschmann MH. Rotating disk heat transfer in a fluid swirling as a forced vortex. Heat and Mass Transfer. 2005; 41(12): 1112-1121. doi: 10.1007/s00231-005-0635-8

18. aus der Wiesche S. Heat transfer from a rotating disk in a parallel air crossflow. International Journal of Thermal Sciences. 2007; 46(8): 745-754. doi: 10.1016/j.ijthermalsci.2006.10.013
19. Hayat T, Khan SB, Sajid M, et al. Rotating flow of a third grade fluid in a porous space with Hall current. Nonlinear Dynamics. 2006; 49(1-2): 83-91. doi: 10.1007/s11071-006-9105-1
20. Yang C, Liao S. On the explicit, purely analytic solution of Von Kármán swirling viscous flow. Communications in Nonlinear Science and Numerical Simulation. 2006; 11(1): 83-93. doi: 10.1016/j.cnsns.2004.05.006
21. Attia HA. Rotating disk flow and heat transfer through a porous medium of a non-Newtonian fluid with suction and injection. Communications in Nonlinear Science and Numerical Simulation. 2008; 13(8): 1571-1580. doi: 10.1016/j.cnsns.2006.05.009
22. Bessaïh R, Boukhari A, Marty P. Magnetohydrodynamics stability of a rotating flow with heat transfer. International Communications in Heat and Mass Transfer. 2009; 36(9): 893-901. doi: 10.1016/j.icheatmasstransfer.2009.06.009
23. Rahman MM, Postelnicu A. Effects of thermophoresis on the forced convective laminar flow of a viscous incompressible fluid over a rotating disk. Mechanics Research Communications. 2010; 37(6): 598-603. doi: 10.1016/j.mechrescom.2010.07.002
24. Abdou MA. New Analytic Solution of Von Karman Swirling Viscous Flow. Acta Applicandae Mathematicae. 2009; 111(1): 7-13. doi: 10.1007/s10440-009-9526-1
25. Turkyilmazoglu M. Analytic approximate solutions of rotating disk boundary layer flow subject to a uniform suction or injection. International Journal of Mechanical Sciences. 2010; 52(12): 1735-1744. doi: 10.1016/j.ijmecsci.2010.09.007
26. Turkyilmazoglu M. Analytic approximate solutions of rotating disk boundary layer flow subject to a uniform vertical magnetic field. Acta Mechanica. 2010; 218(3-4): 237-245. doi: 10.1007/s00707-010-0416-4
27. Rashidi MM, Abelman S, Freidooni Mehr N. Entropy generation in steady MHD flow due to a rotating porous disk in a nanofluid. International Journal of Heat and Mass Transfer. 2013; 62: 515-525. doi: 10.1016/j.ijheatmasstransfer.2013.03.004
28. Alam MS, Chapal Hossain SM, Rahman MM. Transient thermophoretic particle deposition on forced convective heat and mass transfer flow due to a rotating disk. Ain Shams Engineering Journal. 2016; 7(1): 441-452. doi: 10.1016/j.asej.2015.04.005
29. Hayat T, Qayyum S, Imtiaz M, et al. Partial slip effect in flow of magnetite-Fe3O4 nanoparticles between rotating stretchable disks. Journal of Magnetism and Magnetic Materials. 2016; 413: 39-48. doi: 10.1016/j.jmmm.2016.04.025
30. Doh DH, Muthtamilselvan M. Thermophoretic particle deposition on magnetohydrodynamic flow of micropolar fluid due to a rotating disk. International Journal of Mechanical Sciences. 2017; 130: 350-359. doi: 10.1016/j.ijmecsci.2017.06.029
31. Das A, Sahoo B. Flow of a Reiner-Rivlin fluid between two infinite coaxial rotating disks. Mathematical Methods in the Applied Sciences. 2018; 41(14): 5602-5618. doi: 10.1002/mma.5103
32. Kumar A, Tripathi R, Singh R. Von Kármán swirling flow and heat transfer analysis on MHD fluid subject to partial slip and temperature jump conditions. Waves in Random and Complex Media; 2022. doi: 10.1080/17455030.2022.2075044
33. Visuvasam J, Alotaibi H. Analysis of Von Kármán Swirling Flows Due to a Porous Rotating Disk Electrode. Micromachines. 2023; 14(3): 582. doi: 10.3390/mi14030582
34. Ali F, Zaib A, Loganathan K, et al. Scrutinization of second law analysis and viscous dissipation on Reiner-RivlinNanofluid with the effect of bioconvection over a rotating disk. Heliyon. 2023; 9(2): e13091. doi: 10.1016/j.heliyon.2023.e13091
35. Jalili P, Azar AA, Jalili B, et al. Heat transfer analysis in cylindrical polar system with magnetic field: A novel Hybrid Analytical and Numerical Technique. Case Studies in Thermal Engineering. 2022; 40: 102524. doi: 10.1016/j.csite.2022.102524
36. Jalili P, Azar AA, Jalili B, et al. The HAN method for a thermal analysis of forced non-Newtonian MHD Reiner-Rivlin viscoelastic fluid motion between two disks. Heliyon. 2023; 9(6): e17535. doi: 10.1016/j.heliyon.2023.e17535
37. Jalili B, Azar AA, Esmaeili K, et al. A novel approach to micropolar fluid flow between a non-porous disk and a porous disk with slip. Chinese Journal of Physics. 2024; 87: 118-137. doi: 10.1016/j.cjph.2023.11.023
38. Ahmadi Azar A, Jalili B, Jalili P, et al. Investigating the effect of structural changes of two stretching disks on the dynamics of the MHD model. Scientific Reports. 2023; 13(1). doi: 10.1038/s41598-023-48988-4
39. Jalili P, Azar AA, Jalili B, et al. A Novel Analytical Investigation of a Swirling Fluid Flow and a Rotating Disk in the Presence of Uniform Suction. Arabian Journal for Science and Engineering. 2023; 49(8): 10453-10469. doi: 10.1007/s13369-023-08391-7

40. Jalili P, Azar AA, Jalili B, et al. Study of nonlinear radiative heat transfer with magnetic field for non-Newtonian Casson fluid flow in a porous medium. Results in Physics. 2023; 48: 106371. doi: 10.1016/j.rinp.2023.106371
41. Jalili B, Azar AA, Jalili P, et al. Analytical approach for micropolar fluid flow in a channel with porous walls. Alexandria Engineering Journal. 2023; 79: 196-226. doi: 10.1016/j.aej.2023.08.015
42. Jalili B, Azar AA, Jalili P, et al. Investigation of the unsteady MHD fluid flow and heat transfer through the porous medium asymmetric wavy channel. Case Studies in Thermal Engineering. 2024; 61: 104859. doi: 10.1016/j.csite.2024.104859
43. Jalili P, Ahmadi Azar A, Jalili B, et al. A novel technique for solving unsteady three-dimensional brownian motion of a thin film nanofluid flow over a rotating surface. Scientific Reports. 2023; 13(1). doi: 10.1038/s41598-023-40410-3
44. Azar EA, Jalili B, Azar AA, et al. An exact analytical solution of the Emden–Chandrasekhar equation for self-gravitating isothermal gas spheres in the theory of stellar structures. Physics of the Dark Universe. 2023; 42: 101309. doi: 10.1016/j.dark.2023.101309
45. Azar AA, Jalili P, Moziraji ZP, et al. Analytical solution for MHD nanofluid flow over a porous wedge with melting heat transfer. Heliyon. 2024; 10(15): e34888. doi: 10.1016/j.heliyon.2024.e34888
46. Jalili B, Azar AA, Jalili P, et al. Impact of variable viscosity on asymmetric fluid flow through the expanding/contracting porous channel: A thermal analysis. Case Studies in Thermal Engineering. 2023; 52: 103672. doi: 10.1016/j.csite.2023.103672
47. Jalili B, Azar AA, Liu D, et al. Analytical formulation of the steady-state planar Taylor–Couette flow constitutive equations with entropy considerations. Physics of Fluids. 2024; 36(11). doi: 10.1063/5.0239765
48. Ahmadi Azar A, Jalili P, Jalili B, et al. The comprehensive analysis of magnetohydrodynamic Casson fluid flow with rectangular porous medium through expanding/contracting channel. Multidiscipline Modeling in Materials and Structures. 2024; 21(1): 68-97. doi: 10.1108/mmms-07-2024-0179
49. Heidari N, de Montigny M, Azar AA, et al. Solutions of the nonlinear Klein-Gordon equation and the generalized uncertainty principle with the hybrid analytical and numerical method. Nuclear Physics B. 2024; 1009: 116750. doi: 10.1016/j.nuclphysb.2024.116750
50. Xu H, Liao SJ. Series solutions of unsteady MHD flows above a rotating disk. Meccanica. 2006; 41(6): 599-609. doi: 10.1007/s11012-006-9006-x
51. Mehmood A, Ali A, Takhar HS, et al. Unsteady Von Kármán swirling flow: analytical study using the Homotopy Method. International Journal of Applied Mathematics and Mechanics. 2010.
52. Sadiq MA. Serious Solutions for Unsteady Axisymmetric Flow over a Rotating Stretchable Disk with Deceleration. Symmetry. 2020; 12(1): 96. doi: 10.3390/sym12010096
53. Bég OA, Mabood F, Nazrul Islam M. Homotopy Simulation of Nonlinear Unsteady Rotating Nanofluid Flow from a Spinning Body. International Journal of Engineering Mathematics. 2015; 2015: 1-15. doi: 10.1155/2015/272079
54. Schlichting H, Gersten K. Boundary-Layer Theory. Springer Berlin Heidelberg; 2017. doi: 10.1007/978-3-662-52919-5